Available online at www.sciencedirect.com
ScienceDirect
Trans. Nonferrous Met. Soc. China 21(2011) 1491−1497
Transactions of Nonferrous Metals Society of China
www.tnmsc.cn

Microstructure and texture evolution during high-strain-rate superplastic deformation of coarse-grained Mg-Gd-Y-Zr rolled sheet

LI Li[1, 2], ZHANG Xin-ming[1]

1. School of Materials Science and Engineering, Central South University, Changsha 410083, China;
2. Department of Mechanical Engineering, Hunan Institute of Technology, Hengyang 421002, China

Received 4 August 2010; accepted 8 March 2011

Abstract: Microstructure and texture evolution during high-strain-rate superplastic deformation of the rolled Mg-Gd-Y-Zr sheet were investigated. The tensile tests at the strain rate of 0.01 s^{-1} achieved the elongations of 180%−266% in the deformation temperature range of 400−500 °C. Post-deforming microstructures were characterized by optical microscopy, scanning electron microscopy and transmission electron microscopy, while crystallographic orientation information was obtained from macro-texture analysis. The results show that the high strain-rate superplasticity was attributed to class-I dislocation creep accommodated by dynamic recrystallization (DRX). During preheating at 435 °C for 600 s, twinning-induced recrystallization occurred. The initial strain of 80% made original grains fragmented and produced homogenous DRX grains. The interaction between dynamic recrystallization and dynamic precipitation yielded out such a phenomenon that finer DRX grains were often accompanied by denser particles. The macro-texture evolution exhibited some characteristics of the crystal rotation arising from basal slip and prismatic slip despite the occurrence of DRX.

Key words: Mg-Gd-Y-Zr alloy; hot rolling; superplastic mechanism; second phases; texture

1 Introduction

Magnesium alloy products have great potential for aircraft, automotive and electronic industries due to low density and high specific strength [1], but they normally exhibit poor heat resistance. Recent researches show that the addition of gadolinium (Gd) and other rare earths (RE) can remarkably improve the heat resistance of magnesium alloy due to solution hardening and precipitation hardening [2]. The mechanical properties meet the challenge of the heat-resistant components in those fields at elevated temperatures that may be up to 200−300 °C.

In order to overcome the low formability near room temperature, superplastic forming at elevated temperatures has been applied to shaping magnesium alloys into complex geometries [3]. So far, our previous research has been conducted on the low-strain-rate superplasticity of Mg-Gd-Y-Zr rolled sheets [4]. Such superplastic capabilities were fulfilled by grain boundary sliding (GBS) operated within fully recrystallized fine grains. However, microstructure and texture evolution during superplastic deformation have not been investigated attentively, especially for the high-strain-rate superplasticity (HSRSP, higher than 0.01 s^{-1}). Since the HSRSP can enhance the forming efficiency, economize energy, and prevent high temperature oxidation of magnesium alloys, it is always the goal pursued by some researchers. LIN et al [5] applied the most simple and feasible one-step extrusion method to the commercial AZ31 magnesium ingot to result in HSRSP. The processed AZ31 plate possessing a grain size of 1−4 μm exhibited the elongation of 300% at 0.02 s^{-1} and 210 % at 0.1 s^{-1} at 300 °C.

It is widely accepted that the structure superplasticity is associated with a small grain size. The small grain size is desirable in enhancing ductility and increasing the optimum strain rate for superplasticity. However, the initial coarse-grained microstructure achieving a high elongation is expected to save the processing route to obtain fine-grained microstructure. WU [6] found a superplastic-like behavior in a commercial large-grained AZ31 sheet, and the maximum

Foundation item: Project supported by Natural Science Foundation of Hunan Province, China
Corresponding author: LI Li; Tel: +86-734-3452197; E-mail: lileewin@163.com
DOI: 10.1016/S1003-6326(11)60886-8

elongation of 170% to failure was obtained at 0.01 s^{-1} and 500 °C. However, few studies were done on the HSRSP of the magnesium alloys containing rare earth elements with high content. The Mg-Gd-X alloys are able to provide various precipitate phases [2, 7−8] including $\beta''(D0_{19})$, β'(c-base centered orthorhombic), $\beta(Mg_5Gd$, cubic). The β'' and β' are metastable phases, while the β is high temperature stable phase. These second phases are expected to influence the superplastic behavior and microstructural evolution. The aim of this contribution is to explore the microstructure and texture evolution during HSRSP deformation of the coarse-grained Mg-Gd-Y-Zr rolled sheet.

2 Experimental

The experimental material was Mg-9.0Gd-4.0Y-0.4Zr (mass fraction, %) alloy. The as-cast ingot was homogenized at 520 °C for 8 h with subsequent cooling in air. The billets were rolled at 350 °C with intermediate anneal at 500 °C for 15 min. The rollers were heated by a gasoline torch. The reduction in every pass was less than 10%. The sheet with the thickness of 1.3 mm was rolled from original thickness of 4 mm.

The tensile specimens were directly cut from the rolled sheet and had gauge dimensions of 10 mm in length and 3.5 mm in width. The tensile axes was parallel to the rolling direction. The tensile tests were conducted at the strain rate of 0.01 s^{-1} and the temperatures ranging from 400 to 500 °C in air. The tensile specimen was preheated for 600 s prior to the initiation of straining. Three specimens were adopted for each deformation condition.

Optical microscope (OM) was used to examine the grain microstructure. The specimens were etched by a 25% tartaric acid solution for 10 s. The morphologies of second phases and fracture surfaces were examined by scanning electron microscope (SEM). The second phases were identified by energy dispersive X-ray spectrometer (EDS). Transmission electron microscope (TEM) was also used to investigate the post-deformation microstructures. Foils for TEM were prepared by electro-polishing followed by brief low-energy ion beam milling. The final ion-milling step led to an improvement in the foil surface quality without introducing any detrimental artifacts. Macro-texture evolution was determined by measuring incomplete pole figures ($5°\leq\alpha\leq80°$) in the back reflection mode. The (0002), $(10\bar{1}0)$, $(10\bar{1}1)$, $(10\bar{1}2)$ pole figures were measured on the centre plane parallel to the initial sheet surface or the stretched specimen. The LaboTex 3.0 software was used to calculate the orientation distribution function (ODF) at constant section of φ_2=0°−30°. Bunge notations of the Euler angles were used throughout.

3 Results

3.1 Superplastic behaviors

The undeformed and fractured tensile specimens are shown in Fig. 1. For the strain rate of 0.01 s^{-1}, the maximum elongation of 266% was achieved from the specimen tested at 435 °C, in which the diffusional necking took place within the whole gauge length.

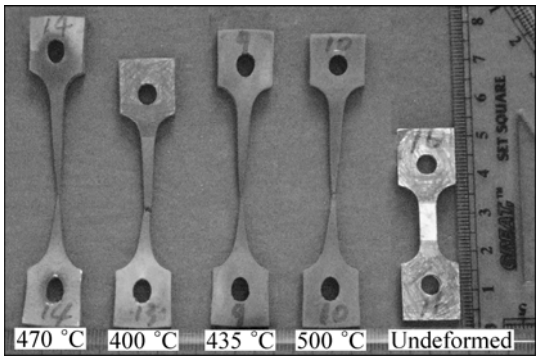

Fig. 1 Undeformed and fractured tensile specimens of rolled Mg-Gd-Y-Zr alloys

Figure 2 shows the true stress—strain curves obtained at various temperatures with the stable strain rate of 0.01 s^{-1}. The true stress was calculated assuming that the specimen was uniformly deformed without necking. It can be observed from Fig. 2 that the true flow stress climbed with strain up to a certain level of true strain, and dropped to the nearly constant value in a range of true strain above the certain level. The apparent strain softening behavior is often associated with dynamic recrystallization (DRX) [9].

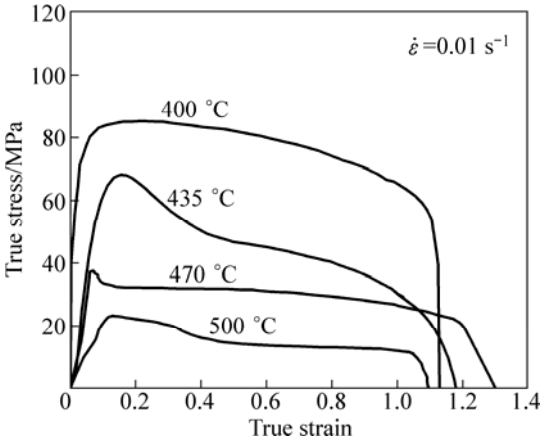

Fig. 2 True stress—strain curves of Mg-G-Y-Zn alloy tested at 0.01 s^{-1}

Figure 3 shows the variation of the averaged elongation to failure as a function of deformation temperature. Each averaged elongation to failure was

obtained from three specimens under the same tensile deformation condition. The elongations were in the range of 180%−266%.

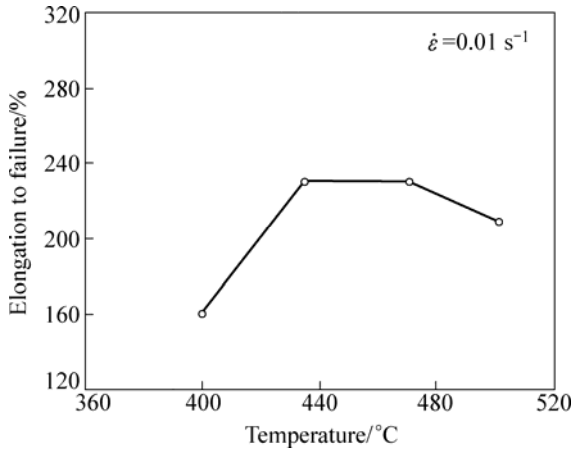

Fig. 3 Variation of elongation to failure as function of tensile temperature

3.2 OM microstructures of initial rolled sheet and post-deformed specimen

The optical microstructure of initial sheet after repeated rolling is shown in Fig. 4(a), where the average grain size was 66 μm. After repeated rolling and annealing, there apparently existed lots of deformation twins and second phases of about 1 μm in both the gain boundaries and the grain interiors.

In order to clarify the influence of preheating on the sheet microstructures, the static annealing at 435 °C for 600 s was conducted on the initial sheet. As shown in Fig. 4(b), no significant change of original grain was observed. However, fine grains occurred within deformation twins, i.e. twinning-induced recrystallization. Figures 4(c) and 4(d) display the OM microstructures for the specimens stretched at 435 °C and 0.01 s^{-1} up to the elongations of 80% and 200%, respectively. As shown in Fig. 4(c), the original grain was fragmented after the tensile deformation of 80%, and the average grain size decreased to 32 μm. It should be emphasized that a homogenous grain size distributed along the gauge length. It is noted in Fig. 4(d) for the larger deformation of 200% that some localized deformation (and therefore localized recrystallization) led to a heterogeneous grain size. A closer inspection of the grain structure in Fig. 4(d) shows that the finer grains were aligned in bands (as indicated by the frame), where the amount of second phases was observed to be relatively large. These facts imply that recrystallization proceeding dynamically during tensile deformation had a close relation to these second phases.

3.3 SEM and TEM microstructures of post- deformed specimen

Figure 5 illustrates SEM microstructures and corresponding EDS profiles at the distance of 2 mm from the fracture surface for the specimen deformed at 435 °C and 0.01 s^{-1}. Figure 5(a) displays SEM photograph of the particle-rich zone, where a large amount of second phases of about 0.4 μm existed in both the gain boundaries and the grain interiors. Moreover, new recrystallized grains of about 3 μm were found within

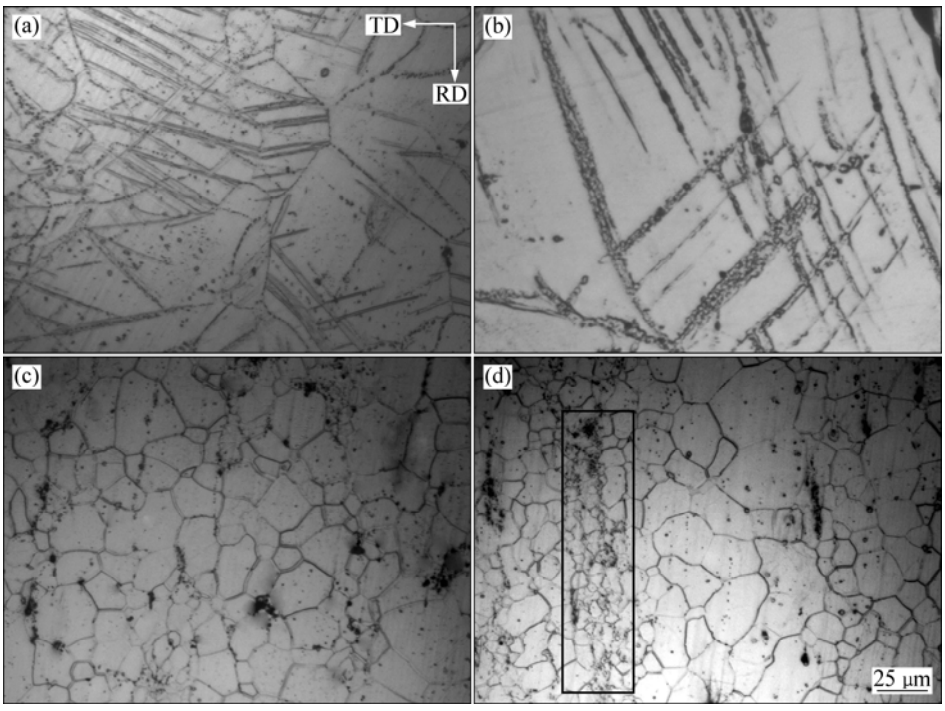

Fig. 4 Optical microstructures of initial sheet after repeated rolling (a), sheets after static annealing at 435 °C for 600 s (b), and post-deformed specimens up to elongation of 80% (c) and 200% (d)

the particle-rich zone. The corresponding EDS in Figs. 5(b) and 5(c) distinguished two types of the second phases in the specimen. The spherical particle (marked by I) was zirconium-rich core because the EDS shows that the spherical particle is enriched in zirconium that never reacts with other elements in the alloy. Examination of more than five times for the irregular-shaped compounds (marked by II) shows that the average mole fractions for Mg and (Gd+Y) were equal to 82.66% and 15.82%. Therefore, the irregular-shaped phase (marked by II) was identified to be $Mg_5(Gd,Y)$, i.e. the β phase [4, 10].

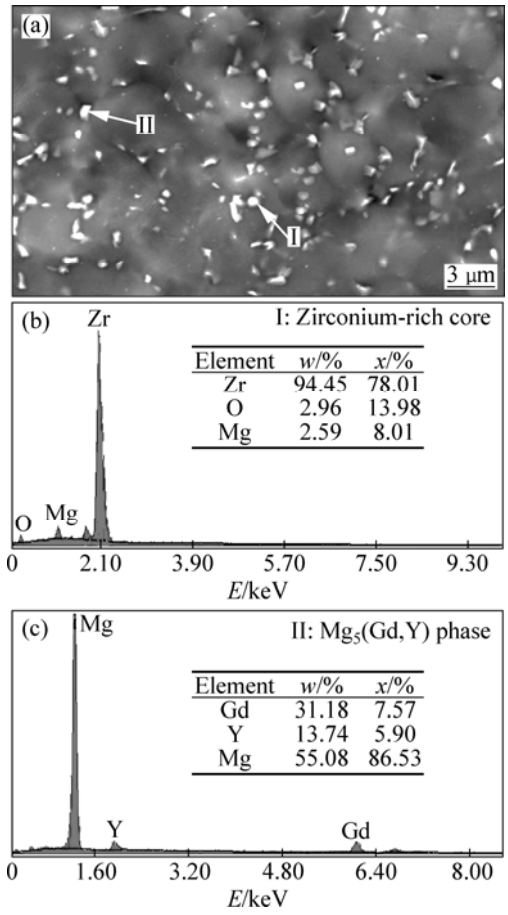

Fig. 5 SEM micrograph of fractured specimen deformed at 435 °C and 0.01 s^{-1} (a) and corresponding compositions of second phases identified by EDS (b, c)

The fracture surface for the specimen deformed at 435 °C and 0.01 s^{-1} is displayed in Fig. 6, where the fracture mode was a basically intragranular manner by tearing fracture mode. Much dimples with tearing edges appeared on fracture surface, which originated from dislocation creep [11]. At the same time, there were some second phases within these dimples.

Figure 7 shows TEM microstructures of the fractured specimen tested at 435 °C and 0.01 s^{-1}. In some grains interiors, dislocation walls were observed in the region adjacent to the second particles. It has been recognized that dynamic recrystallization (DRX) proceeds continuously, when dislocations remain in the recrystallized grains [12]. Obviously, new recrystallized grains were formed finally at the base of subgrain boundaries and particles of second phases. The β phases hindered DRX by exerting a significant pinning effect on grain (subgrain) boundaries.

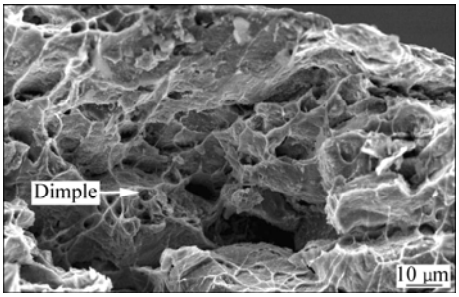

Fig. 6 SEM image of fracture surface for specimen deformed at 435 °C and 0.01 s^{-1}

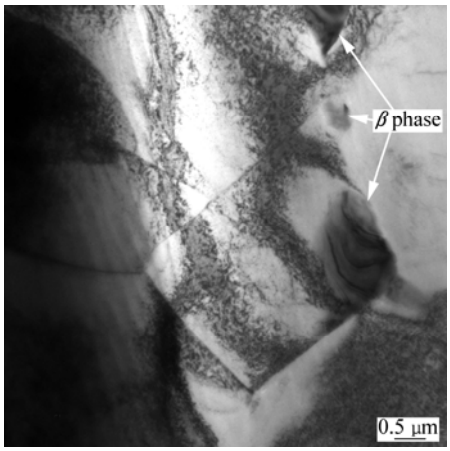

Fig. 7 TEM image of fractured specimen deformed at 435 °C and 0.01 s^{-1}

3.4 Evolution of macro-texture

Figure 8 presents the ODFs at the sections of φ_2=0°−30° of the initial sheet and necking regions of the tensile specimens at different strain levels. As indicated in Fig. 8(a), two dominant texture components were involved within the initial sheet, i.e. quasi-basal fiber (Quasi-BF deviates about 15° from the ideal BF (Φ=0°)) and prismatic fiber (PF, i.e. Φ=90°). The texture at the strain of 80% is shown in Fig. 8(b). The *c*-axis of the quasi-BF was aligned parallel to that of the ideal BF. The fiber tended to concentrate on the $\langle 10\bar{1}0\rangle$ direction and $\langle 11\bar{2}0\rangle$ direction and were evolved as the texture *g*1 $\{0001\}\langle 10\bar{1}0\rangle$ and *g*2 $\{0001\}\langle 11\bar{2}0\rangle$, respectively. Moreover, the quasi-BF was evolved into *g*3 (φ_1, Φ, φ_2)=(90°, 15°, 15°) by the rotation around *c*-axis. Meanwhile, as suggested in the section of φ_2=0−30° in Fig. 8(b), the PF in the initial sheet was weakened obviously. Figure 8(c) presents the ODFs of the deformed specimen at the strain of 200%, where the texture

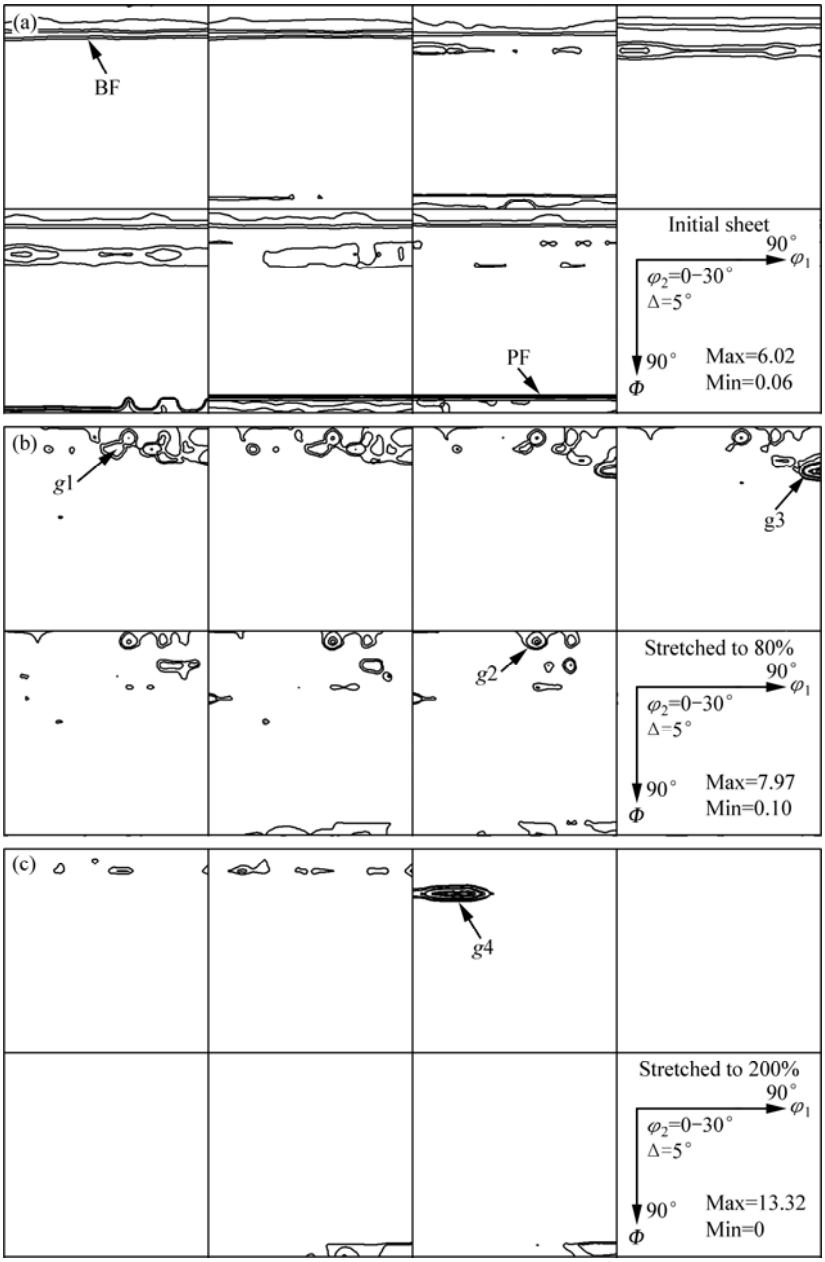

Fig. 8 Macro-texture described by orientation distribution function (φ_2=0−30°) of initial sheet and specimens deformed at 435 °C and 0.01 s^{-1}: (a) Initial sheet; (b) Stretched to 80%; (c) Stretched to 200%

intensity was strengthened and only one texture component yielded out, i.e. *g*4 (φ_1, Φ, φ_2)=(30°, 15°, 10°). A full summary of all ODFs at different stages indicates that the texture gradually concentrated on a certain direction and tended to be stronger with the strain level.

4 Discussion

TAN et al [13] found that the optimum deformation conditions of Mg-3Al-1Zn were at temperature of 450 °C and strain rate of 2×10^{-4} s^{-1}, attaining a maximum elongation of 265%. Therefore, the studied alloy has great potential to achieve the high-strain-rate superplastic deformation compared with Mg-3Al-1Zn alloy.

Our previous research indicated [4] that the strain rate sensitivity, i.e. *m*-value at 0.01 s^{-1} was about 0.31. This result suggests that the class-I dislocation creep, which is associated with an elongation of about 300% and a *m*-value of 0.31, may play an important role in the superplastic deformation [14].

In order to understand the mechanism during superplastic process, the superplastic deformation activation energy *Q* was calculated under constant strain rate by the following equation [15]:

$$Q = nR\frac{\partial \ln \sigma}{\partial (1/T)} \quad (1)$$

where σ is the flow stress; n is the stress exponent (n=1/m); R is the molar gas constant (R=8.314 J/K); T is the thermodynamic temperature; $\partial \ln\sigma / \partial(1/T)$ is estimated from the slope of the curve in Fig. 9. The activation energy was determined to be 178 kJ/mol, which is higher than the activation energy for grain boundary self diffusion (75 kJ/mol) or lattice diffusion (134 kJ/mol) of magnesium alloys [16].

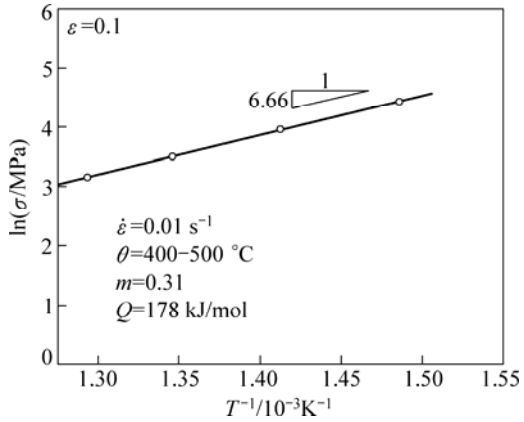

Fig. 9 Activation energy curves of lnσ vs. 1/T of HSRSP for rolled Mg-Gd-Y-Zr sheet

The recrystallization can be divided into static recrystallization and dynamic recrystallization. The twinning-induced recrystallization belongs to static recrystallization. The twinning boundary can activate the occurrence of the non-basal slip system due to the stress concentration introduced by the dislocation pile-ups at the vicinity of twin boundary [17]. Therefore, the activation and rearrangement of dislocation within twin stored energy for the subsequent static recrystallization (see Fig. 4(b)).

The second particles have two important effects on DRX: 1) The interaction between the second particles and dislocation during deformation increases the driving force for recrystallization; 2) Fine second particles, particularly if closely spaced, may exert a significant pinning effect on grain boundaries. The first effect tends to promote recrystallization, whereas the second tends to hinder recrystallization. For magnesium alloys which possess limited slip systems, low stacking fault energy and high grain boundary diffusion rate [18], dislocation pile-up stimulates the forming of sub-grain boundaries that signifies the onset of DRX. Thus, DRX occurs readily in magnesium and its alloys.

TAN et al [13] proved that DRX proceeded continuously through the conversion of low angle boundaries into high angle boundaries, and that the presence of precipitates was not essential for DRX in the AZ31 magnesium alloy. Hot deformation involving hard particles led to continuing dislocation pile-up at the region adjacent to the phase interfaces. The precipitation behavior of Mg-Gd-Y-Zr were examined in Ref. [19], and the precipitating sequence was $\beta''\rightarrow\beta'\rightarrow\beta_1\rightarrow\beta$. However, at elevated temperatures of 430−450 °C, the irregular-shaped β was deformable and the strain could be partly transferred from the matrix to β phase [10]. It follows that the pile-up of dislocations can not occur on the phase interfaces. Therefore, the hindering effect of second particles on DRX gained the advantage over the promoting effect. In more details, the initial deformation led to the onset of dislocation walls with low angle boundaries that provided the favorable positions for precipitating. When the low angle boundaries converted into the high angle boundaries, the second phases began to coarsen and pin the dynamic recrystallized grain boundaries. As a result, the interaction between dynamic recrystallization and dynamic precipitation yields out the resultant phenomenon that finer DRX grains were often accompanied by higher dense particles (in Fig. 4(c) and Fig. 5(a)).

Since the superplastic deformation was dominated by the class-I dislocation creep, the evolution of macro-texture is expected to be explained by the crystal rotation arising from dislocation slip. Firstly, the basal slip that is the most active slip system in magnesium alloys ought to strengthen the BF, especially in the early stage of deformation [20]. So the basal slip accounted for the transition from quasi-BF to ideal-BF (see Fig. 8(b)). Secondly, for the high temperature deformation, non-basal slip systems can be activated readily, which is always accompanied by the DRX. The phenomena in Fig. 8(b) that the BF fiber tended to concentrate on the $\langle 10\bar{1}0\rangle$ and $\langle 11\bar{2}0\rangle$ should be associated with the DRX since DRX often yields a texture subtle variation, i.e. the 30°[0001] preference [21]. Thirdly, the formation of g3 and g4, as observed in Figs. 8(b) and (c), was attributable to the prismatic slip, due to the recognition that the slip system gives rise to rotations around c-axis [22]. It is demonstrated that the texture exhibited some characteristics of the crystal rotation arising from basal slip and prismatic slip despite the occurrence of DRX.

5 Conclusions

1) High-strain-rate superplasticity and micro-structure of the rolled Mg-Gd-Y-Zr sheet with an initial grain size of 66 μm were investigated. The material exhibited the elongation of 180%−266% at the strain rate of 0.01 s^{-1} and the temperatures ranging from 400 °C and 500 °C. The predominant superplastic mechanism was class-I creep accommodated by continuously dynamic recrystallization.

2) Twinning-induced recrystallization occurred during the preheating at 435°C for 600 s. The interaction between dynamic recrystallization and dynamic

precipitation yielded out such a phenomenon that finer DRX grains are often accompanied by denser particles. The hindering effect of second particles on DRX gained the advantage over the promoting effect.

3) During high-strain-rate superplastic deformation, the texture evolution manifested some characteristics of the crystal rotation arising from basal slip and prismatic slip despite the occurrence of DRX.

References

[1] LUO A A. Recent magnesium alloy development for elevated temperature applications [J]. Int Mater Rev, 2004, 49(1): 13−30.

[2] XIAO Yang, ZHANG Xin-ming, CHEN Bu-xiang, DENG Zhen-zhen. Mechanical properties of Mg-9Gd-4Y-0.6Zr alloy [J]. Transactions of Nonferrous Metals Society of China, 2006, 16(3): 1169−1172.

[3] BLANDIN J J. Superplastic forming of magnesium alloys: Production of microstructures, superplastic properties, cavitation behaviour [J]. Superplasticity in Advanced Materials, 2007, 551−552: 211−217.

[4] LI L, ZHANG X, DENG Y, TANG C. Superplasticity and microstructure in Mg-Gd-Y-Zr rolled sheet [J]. J Alloy Compd, 2009, 485: 295−299.

[5] LIN H K, HUANG J C. High strain rate and/or low temperature superplasticity in AZ31 Mg alloys processed by simple high-ratio extrusion methods [J]. Mater Trans, 2002, 43(10): 2424−2432.

[6] WU X, LIU Y, HAO H. High strain rate superplasticity and microstructure study of a magnesium alloy [J]. Materials Science Forum, 2001, 357−359: 363−370.

[7] MORDIKE B L. Creep-resistant magnesium alloys [J]. Materials Science and Engineering A, 2002, 324(1−2): 103−112.

[8] SMOLA B, STULÍOVÁ I, PELCOVÁ J, MORDIKE B L. Significance of stable and metastable phases in high temperature creep resistant magnesium-rare earth base alloys [J]. J Alloy Compd, 2004, 378(1−2): 196−201.

[9] YANG X, MIURA H, SAKAI T. Dynamic evolution of new grains in magnesium alloy AZ31 during hot deformation [J]. Mater Trans, 2003, 44(1): 197−203.

[10] ZHANG X, LI L, DENG Y, ZHOU N. Superplasticity and microstructure in Mg-Gd-Y-Zr alloy prepared by extrusion [J]. J Alloy Compd, 2009, 481(1−2): 296−300.

[11] WATANABE H. Low temperature superplasticity in a ZK60 magnesium alloy [J]. Materials Transactions JIM, 1999, 40(8): 809−814.

[12] MOHRI T, MABUCHI M, NAKAMURA M, ASAHINA T, IWASAKI H, AIZAWA T, HIGASHI K. Microstructural evolution and superplasticity of rolled Mg-9Al-1Zn [J]. Materials Science and Engineering A, 2000, 290(1−2): 139−144.

[13] TAN J C, TAN M J. Dynamic continuous recrystallization characteristics in two stage deformation of Mg-3Al-1Zn alloy sheet [J]. Materials Science and Engineering A, 2003, 339(1−2): 124−132.

[14] WATANABE H, TSUTSUI H, MUKAI T, KOHZU M, TANABE S, HIGASHI K. Deformation mechanism in a coarse-grained Mg-Al-Zn alloy at elevated temperatures [J]. Int J Plast, 2001, 17(3): 387−397.

[15] WU X, LIU Y. Superplasticity of coarse-grained magnesium alloy [J]. Scr Mater, 2002, 46(4): 269−274.

[16] FROST H J, ASHBY M F, Deformation mechanism map [M]. New York: Pergamon Press, 1982: 44.

[17] YE Cheng-wu, LIU Zhi-yi, ZHANG Kun, ZHENG Qing-chun. Twinning during hot compression of ZK30 + 0.3Yb magnesium alloy [J]. Transactions of Nonferrous Metals Society of China, 2005, 15(4): 884−888.

[18] ION S E, HUPHREYS F J, WHITE S H. Dynamic recrystallisation and the development of microstructure during the high temperature deformation of magnesium [J]. Acta Mater, 1982, 30(10): 1909−1919.

[19] NIE J F, MUDDLE B C. Precipitation in magnesium alloy WE54 during isothermal ageing at 250 °C [J]. Scripta Materialia, 1999, 40(10): 1089−1094.

[20] WATANABE H. Mechanical properties and texture of a superplastically deformed AZ31 magnesium alloy [J]. Materials Science and Engineering A, 2008, 477(1−2): 153−161.

[21] BEAUSIR B, SUWAS S, TOTH L S, NEALE K W, FUNDENBERGER J J. Analysis of texture evolution in magnesium during equal channel angular extrusion [J]. Acta Mater, 2008, 56(2): 200−214.

[22] AGNEW S R, YOO M H, TOME C N. Application of texture simulation to understanding mechanical behavior of Mg and solid solution alloys containing Li or Y [J]. Acta Mater, 2001, 49(20): 4277−4289.

粗晶 Mg-Gd-Y-Zr 热轧板材高速超塑性变形中的微观结构与织构演变

李 理[1,2]，张新明[1]

1. 中南大学 材料科学与工程学院，长沙 410083；

2. 湖南工学院 机械工程系，衡阳 421002

摘 要：研究 Mg-Gd-Y-Zr 热轧板高速超塑性变形过程中的微观结构与织构演变。在应变速率 0.01 s^{-1}、变形温度 400−500 °C 的条件下，高温拉伸获得伸长率为 180%−266%。变形后的微观结构采用光学显微镜、扫描电子显微镜及透射电子显微镜进行表征；变形后的晶体取向信息采用宏观织构测试分析获得。研究结果表明：高速超塑性是通过动态再结晶协调下的第一类位错蠕变来实现的。合金变形前在 435 °C 预热 600 s 后，观察到了孪晶诱发的再结晶现象；当变形量为 80%时，初始的晶粒细化导致均匀的动态再结晶组织。动态再结晶与动态析出的交互作用使得较细的晶粒与较高密度的第二相粒子相伴存在；尽管发生动态再结晶，宏观织构的演变依然表现出基面滑移与柱面滑移导致的晶体转动特征。

关键词：Mg-Gd-Y-Zr 合金；热轧；超塑性机制；第二相；织构

(Edited by YANG Hua)